Rapid X-ray Declines in Swift Gamma Ray Burst Lightcurves Explained by A Highly Radiative Blast Wave Phase

Charles D. Dermer[1]

ABSTRACT

X-ray lightcurves of GRBs show rapid declines some hundreds of seconds after the burst trigger in $\approx 30\%$ of GRBs in the Swift sample. Treating the standard blast model in a uniform circumburst medium, we show that if GRBs accelerate ultra-high energy cosmic rays through a Fermi mechanism, then the hadronic component can be rapidly depleted by means of photopion processes on time scales $\sim 10^2$ – 10^4 s after the GRB explosion. While discharging the hadronic energy in the form of ultra-high energy cosmic ray neutrons and escaping cosmic ray ions, the blast wave will go through a strongly radiative phase that drives the mean blast wave Lorentz factor to a radiative asymptote. This process is argued to cause the steep declines observed with Swift in the X-ray light curves of GRBs, implying that GRB sources showing rapid X-ray declines take place in rather dense media, with $n \gtrsim 10^2$ cm^{-3} out to $\gtrsim 10^{17}$ cm.

Subject headings: gamma rays: bursts — stars: winds, outflows — nonthermal radiation physics

1. Introduction

Important clues to the nature of GRBs are encoded in their light curves. Swift observations are giving a new data base of GRB light curves, consisting of a BAT light curve in the 15 – 150 keV range followed after slewing within ≈ 100 s by a detailed 0.3 – 10 keV XRT X-ray light curve and by UVOT monitoring (Gehrels et al. 2004). Extrapolating the BAT light curve to the XRT range gives $\sim$ keV X-ray light curves since the trigger. O'Brien et al. (2006) present a catalog of the combined 0.3 – 10 keV light curves of 40 GRBs, of which 14 or so have measured redshifts, $\approx 30\%$ display rapid X-ray declines, and an additional $\approx 30\%$ display features unlike simple blast wave model predictions. About one-half the sample shows X-ray flares or short timescale structure.

[1]E. O. Hulburt Center for Space Research, Code 7653 Naval Research Laboratory, Washington, D.C. 20375-5352; dermer@gamma.nrl.navy.mil

A combined leptonic-hadronic GRB model is considered in this paper. The analysis follows the standard blast wave model (e.g., Mészáros 2006). We show that if GRBs accelerate cosmic rays to ultra-high energies, then for a certain class of GRBs, the GRB blast wave will become strongly radiative during the early afterglow and, arguably, will exhibit rapid X-ray declines. This class of GRBs is defined by a range of blast wave and environmental parameters, namely initial Lorentz factors $\Gamma_0 \sim 100$ – 300, apparent total energy releases $\gtrsim 10^{54}$ ergs, and surrounding medium density $n \gtrsim 10^2$ cm^{-3}, assumed to be proton dominated. The blast wave microphysical parameters ϵ_e, ϵ_B must both be $\gtrsim 0.1$.

For these GRBs, Fermi processes in the blast wave are assumed to accelerate proton and ions, like they do electrons, to ultrarelativistic energies. Photopion interactions by the ultrarelativistic ions with the internal synchrotron photons make a source of escaping neutrons, neutrinos and cascade γ-rays. Proton synchrotron photons provide a weaker component. This interpretation explains CGRO observations on GRB 940217 and GRB 941017, and makes predictions for correlated Swift and GLAST observations, IceCube, ground-based Cherenkov telescopes, and Auger.

2. Analysis

The energy flux $\Phi_E = dE/dAdt = \nu F_\nu = f_\epsilon = L_*/4\pi d_L^2$, where $d_L = 10^{28} d_{28}$ cm is the luminosity distance, and the source luminosity $L_* = 4\pi x^2 c u'_0 \Gamma^2$. We employ the relations $\epsilon' = h\nu'/m_e c^2 \cong (1+z)\epsilon/2\Gamma$ and $x \cong 2\Gamma^2 c t_v/(1+z)$, where t_v is a characteristic measured variability time scale and primes denote quantities in the comoving fluid frame. Thus the comoving energy density $u'_{\epsilon'} = m_e c^2 \epsilon'^2 n'_{ph}(\epsilon') \cong k d_L^2 f_\epsilon / c x^2 \Gamma^2$, where $k \gtrsim 1/3$ gives the kinematic minimum photon energy density that produces a received spectrum with νF_ν flux $= f_\epsilon$ (Dermer 2004). The GRB spectrum is approximated by the form

$$n'_{ph}(\epsilon') = \frac{k d_L^2 f_{\epsilon_{pk}}}{c x^2 \Gamma^2 m_e c^2} \, \frac{[u^a H(1-u) + u^b H(u-1)]}{\epsilon'^{\,2}} \,, \tag{1}$$

where $u = \epsilon/\epsilon_{pk} = \epsilon'/\epsilon'_{pk}$, $f_{\epsilon_{pk}} = 10^{-6} f_{-6}$ ergs cm^{-2} s^{-1} is the peak νF_ν flux at the νF_ν peak photon energy ϵ_{pk}, $a > 0$ and $b < 0$ are the νF_ν indices, and the Heaviside function $H(r)$ restricts the lower and upper branches of the spectra to their respective ranges.

2.1. Photopion Losses

The energy-loss rate to photopion production on the GRB spectral radiation field is

$$r_{\phi\pi} = t'^{-1}_{\phi\pi}(\gamma'_p) \cong \frac{c}{2\gamma'^2_p}\int_0^\infty d\epsilon'\ \frac{n'_{ph}(\epsilon')}{\epsilon'^2}\int_0^{2\gamma'_p\epsilon'} d\epsilon'_r\ \epsilon'_r\sigma^K_{\phi\pi}(\epsilon'_r)$$

$$\approx \frac{k\hat\sigma d_L^2 f_{\epsilon_{pk}}}{x^2\Gamma^2 m_e c^2\epsilon_{pk}}\ \{H(1-y)[\frac{y^2}{3-a} - \frac{2y^{a-1}}{(3-a)(a-1)} + \frac{1}{a-1}]$$

$$+ [\frac{\max(1,y)^{b-1}}{1-b} - \frac{y^2\max(1,y)^{b-3}}{3-b}]\}\ , \tag{2}$$

after substituting eq. (1), where $y = \epsilon'_{thr}/2\gamma'_p\epsilon'_{pk}$. Here we use the approximation of Atoyan & Dermer (2003), where the product of the photopion cross section and inelasticity is $\sigma^K_{\phi\pi}(\epsilon'_r) = \hat\sigma \cong 70\ \mu$b for $\epsilon'_r \gtrsim \epsilon'_{thr} \cong 400$, and vanishes for $\epsilon'_r \leq \epsilon'_{thr}$.

The asymptotes of eq. (2) are

$$t'^{-1}_{\phi\pi}(\gamma_p) \cong K_{\phi\pi}(\bar\gamma_p)\ \begin{cases} y^{b-1}, & y \geq 1 \\ \frac{(3-b)(a-b)}{2(a-1)}\ , & y \ll 1,\ 1 \leq a \leq 3 \\ \frac{(1-b)(3-b)}{(3-a)(1-a)}y^{a-1}, & y \ll 1,\ 0 \leq a \leq 1 \end{cases} \tag{3}$$

where $y = 1$ defines the Lorentz factor $\bar\gamma'_p$ of protons that interact primarily with internal synchrotron photons at the νF_ν peak frequency ϵ'_{pk}. We call this the peak cosmic-ray proton energy $\bar E_p = m_p c^2\bar\gamma_p = m_p c^2\Gamma\bar\gamma'_p$, as it is the characteristic energy of protons that would escape from the blast wave with Lorentz $\bar\gamma_p$ factor as measured by a local observer. Thus

$$\bar E_p = \frac{m_p c^2\Gamma^2\epsilon'_{thr}}{(1+z)\epsilon'_{pk}} \cong \frac{1.7\times10^{16}(\Gamma/300)^2}{(\frac{1+z}{2})\epsilon_{pk}}\ \text{eV}\ , \tag{4}$$

and

$$K_{\phi\pi}(\bar\gamma_p)\ = \frac{2k\hat\sigma d_L^2 f_{\epsilon_{pk}}}{x^2\Gamma^2 m_e c^2\epsilon'_{pk}(1-b)(3-b)}$$

$$\cong \frac{1.1\times10^{-6}kd_{28}^2 f_{-6}}{(1-b)(3-b)(1+z)x_{16}^2(\Gamma/300)\epsilon_{pk}}\ \text{s}^{-1}\ , \tag{5}$$

and $x = 10^{16}x_{16}$ cm.

2.2. Adiabatic Blast Wave

A blast wave with apparent *total* isotropic energy release $E_0 = 10^{54} E_{54}$ ergs and coasting Lorentz factor $\Gamma_{300} = \Gamma_0/300$ that sweeps through a uniform surrounding medium with proton density $n_0 = 100 n_2$ cm^{-3} will slow down on the deceleration length scale

$$x_d = \frac{3E_0}{4\pi m_p c^2 n_0 \Gamma_0^2} \cong 2.6 \times 10^{16} (\frac{E_{54}}{n_2 \Gamma_{300}^2})^{1/3} \text{ cm} \tag{6}$$

(Mészáros & Rees 1993). A relativistic adiabatic blast wave decelerates according to the relation

$$\Gamma = \Gamma_0 / \sqrt{1 + 2(x/x_d)^3} \tag{7}$$

(Böttcher & Dermer 2000), from which can be derived the asymptotes

$$\frac{x}{x_d} = \begin{cases} \tau, & \tau \ll 1 \\ (2\tau)^{1/4}, & \tau \gg 1 \end{cases} \tag{8}$$

and

$$\frac{\Gamma}{\Gamma_0} = \begin{cases} 1, & \tau \ll 1 \\ 2^{-7/8} \tau^{-3/8}, & \tau \gg 1 \end{cases} , \tag{9}$$

where dimensionless time $\tau = t/t_d = t'/t'_d$, the deceleration time

$$t_d = \frac{(1+z)x_d}{\Gamma_0^2 c} \cong 9.6(1+z)(\frac{E_{54}}{n_2 \Gamma_{300}^8})^{1/3} \text{ s} , \tag{10}$$

and

$$t_d'^{-1} = (\frac{x_d}{\Gamma_0 c})^{-1} \cong 3.5 \times 10^{-4} (\frac{n_2 \Gamma_{300}^5}{E_{54}})^{1/3} \text{ s}^{-1} . \tag{11}$$

The available time in the comoving frame is

$$t'_{ava} = t'_d \begin{cases} \tau, & \tau \ll 1 \\ (2^{17/8}/5)\tau^{5/8} \cong 0.872 \tau^{5/8}, & \tau \gg 1 \end{cases} , \tag{12}$$

2.3. Blast Wave Physics

We treat the photopion process in the fast cooling regime (Sari et al. 1998). The minimum Lorentz factor $\gamma_{min} = \epsilon_e f_p m_p \Gamma/m_e$, where $f_p = (p-2)/(p-1)$ and $2 < p < 3$. The emission detected by Swift is assumed to be nonthermal synchrotron radiation. The mean magnetic field in the fluid frame is $B = bB_{cr} = \sqrt{32\pi m_p c^2 n_0 \epsilon_B}\Gamma \cong 0.4\sqrt{\epsilon_B n_0}\ \Gamma$ G $\cong 370\sqrt{\epsilon_{B-1} n_2}\ \Gamma_{300}(\Gamma/\Gamma_0)$ G, where $B_{cr} = m_e^2 c^3/e\hbar \cong 4.414 \times 10^{13}$ G, and the minimum frequency for the mean observed synchrotron photon energy from electrons with γ_{min} is

$$\epsilon_{min} \cong \frac{\Gamma b \gamma_{min}^2}{1+z} \cong \frac{0.85\sqrt{\epsilon_{B-1} n_2}\epsilon_{e-1}^2 f_{5/2}^2 \Gamma_{300}^4 (\Gamma/\Gamma_0)^4}{1+z} \ . \tag{13}$$

The cooling Lorentz factor $\gamma_c = 3m_e(1+z)/16 m_p \sigma_{\rm T} \epsilon_B n_0 \Gamma^3 c t_d \tau$, and the cooling frequency

$$\epsilon_c \cong \frac{2.3 \times 10^5 (1+z)}{(\epsilon_B n_0)^{3/2} \Gamma^4 t_d^2 \tau^2} \ \cong \ \frac{1.0 \times 10^{-8} \Gamma_{300}^{4/3} (\Gamma/\Gamma_0)^{-4}}{\epsilon_{B-1}^{3/2} n_2^{5/6} (1+z) E_{54}^{2/3} \tau^2} \ . \tag{14}$$

Comparing eqs. (13) and (14) shows that we are in the strong cooling regime, $\epsilon_c < \epsilon_{min}$, when

$$\tau \lesssim 7 \times 10^5 \ (\epsilon_{e-1}\epsilon_{B-1} f_{5/2})^2 n_2^{4/3} E_{54}^{2/3} \Gamma_{300}^{8/3} \ . \tag{15}$$

The received energy flux at ϵ_{pk} from the fast-cooling blast wave is

$$f_{\epsilon_{pk}} \cong \frac{\Gamma^2}{4\pi d_L^2} \ (\frac{4}{3} c \sigma_{\rm T} U_B) \ \gamma_{min}^3 N_e'(\gamma_{min}; x) \ , \tag{16}$$

where $U_B = B^2/8\pi$ is the magnetic-field energy density in the comoving frame. For the fast-cooling regime, $N_e'(\gamma_{min}) \cong N_e(x)\gamma_c \gamma_{min}^{-2}$ and $N_e(x) = 4\pi n_0 x^3/3$. Thus

$$f_{\epsilon_{pk}}(10^{-6} \text{ ergs cm}^{-2} \text{ s}^{-1})$$

$$\cong 2.7 \ \frac{\epsilon_{e-1} f_{5/2} n_2^{1/3} E_{54}^{2/3} \Gamma_{300}^{8/3}}{d_{28}^2} \begin{cases} \tau^2, & \tau \lesssim 1 \\ (2\tau)^{-1}, & \tau \gg 1 \end{cases} \ . \tag{17}$$

2.4. Timescale Comparison

The measured peak photon energy is

$$\epsilon_{pk} \cong \frac{0.85\sqrt{\epsilon_{B-1}n_2}\epsilon_{e-1}^2 f_{5/2}\Gamma_{300}^4}{1+z}\begin{cases}1, & \tau \ll 1\\ 0.09\tau^{-3/2}, & \tau \gg 1\end{cases} \tag{18}$$

Substituting eqs. (8), (9), and (18) into eq. (3) gives the comoving photopion energy-loss rate

$$t'^{-1}_{\phi\pi}(\bar{E}_p) \cong \frac{5.2\times 10^{-7} k n_2^{1/2}\ \mathrm{s}^{-1}}{(1-b)(3-b)\Gamma_{300}^2\epsilon_{B-1}^{1/2}\epsilon_{e-1}}\begin{cases}1, & \tau \lesssim 1\\ 2^{23/8}\tau^{3/8}, & \tau \gg 1\end{cases} \tag{19}$$

at the characteristic energy

$$\bar{E}_p(\mathrm{eV}) \cong \frac{4\times 10^{16}}{\sqrt{\epsilon_{B-1}n_2}\epsilon_{e-1}^2 f_{5/2}\Gamma_{300}^2}\begin{cases}1, & \tau \lesssim 1\\ 3.4\tau^{3/4}, & \tau \gg 1\end{cases} \tag{20}$$

of an escaping cosmic ray measured in the local source frame.

Because a significant energy gain by a particle can take place through Fermi acceleration mechanisms on times not shorter than the Larmor time $t'_{\rm L} = mc^2\gamma'_p/eBc = (mc/eB)(\gamma/\Gamma)$ (Rachen & Mészáros 1998), the acceleration time scale in the proper frame can be written as $t'_{acc} = \zeta_{acc}t'_{\rm L}$, $\zeta_{acc} \gg 1$. Hence the acceleration rate r_{acc} at the peak cosmic-ray proton energy is given by

$$t'^{-1}_{acc}(\bar{E}_p) \cong 25\ \mathrm{s}^{-1}\ \frac{n_2\epsilon_{B-1}\Gamma_{300}^4\epsilon_{e-1}^2 f_{5/2}}{\zeta_{acc}}\begin{cases}1, & \tau \lesssim 1\\ \frac{1}{11.4\tau^{3/2}}, & \tau \gg 1\end{cases} \tag{21}$$

The acceleration rate for $10^{20}E_{20}$ eV cosmic ray protons is

$$t'^{-1}_{acc}(E_{20}) \cong \frac{1.1\times 10^{-3}\mathrm{s}^{-1}\sqrt{\epsilon_{B-1}n_2}}{(\zeta_{acc}/10)\,E_{20}}\frac{\Gamma_{300}^2}{(1+2^{7/8}\tau^{3/8})^2} \tag{22}$$

The mean escape rate using the Bohm diffusion approximation is given by $t'_{esc} = \langle x\rangle^2/2\kappa_{\rm B}$, where $\kappa_{\rm B} = c^2t'_{\rm L}/3$ is the diffusion coefficient, the characteristic dimension $\langle x\rangle$

is the shell width $\Delta' = f_\Delta x/\Gamma$, and $f_\Delta \cong 1/12$ for the width of the shocked fluid shell swept from the circumburst medium by an adiabatic relativistic blast waves (e.g., Panaitescu & Mészáros 1999). Thus the escape rate is

$$t'^{-1}_{esc} \cong \frac{2cE_p\Gamma}{3eBf_\Delta^2 x_d^2}\ \frac{1}{(x/x_d)^2}\ . \tag{23}$$

The escape rate for protons with characteristic energy $\bar{E}_p$, eq. (20), is

$$t'^{-1}_{esc}(\bar{E}_p) \cong \frac{5\times 10^{-7}\ \mathrm{s}^{-1}}{\epsilon_{B-1} n_2^{1/3}\epsilon_{e-1}^2 f_{5/2}\Gamma_{300}^{2/3}} \begin{cases} \tau^{-2}, & \tau \lesssim 1 \\ 2.4\tau^{1/4}, & \tau \gg 1 \end{cases} . \tag{24}$$

The escape rate for $10^{20}E_{20}$ eV cosmic ray protons is

$$t'^{-1}_{esc}(E_{20}) \cong \frac{1\times 10^{-3} E_{20} n_2^{1/6}\Gamma_{300}^{4/3}\ \mathrm{s}^{-1}}{\sqrt{\epsilon_{B-1}}E_{54}^{2/3}} \begin{cases} \tau^{-2}, & \tau \lesssim 1 \\ (2\tau)^{-1/2}, & \tau \gg 1 \end{cases} . \tag{25}$$

We also have the Hillas (1984) condition that the Larmor radius $r_{\rm L} = (mc^2/eB)(\gamma/\Gamma) \lesssim \Delta' \cong f_\Delta x/\Gamma$, limiting acceleration to protons with energies less than

$$E_p^{\rm H}(10^{20}\ \mathrm{eV}) = 2.4\ \epsilon_{B-1}^{1/2} n_2^{1/6}\Gamma_{300}^{1/3}E_{54}^{1/3} \begin{cases} \tau, & \tau \lesssim 1 \\ \frac{\tau^{-1/8}}{2^{5/8}}, & \tau \gg 1 \end{cases} , \tag{26}$$

using the asymptotes, eqs. (8) and (9). Note the slow late-time decline $E_p^{\rm H} \propto t^{-1/8}$ when $\tau \gg 1$ (Vietri 1998; Böttcher & Dermer 1998). Thus we see that standard parameter values allow Fermi acceleration of protons to ultra-high energies in GRB blast waves, making GRBs a leading candidate for UHECR production.

2.5. Proton Synchrotron Radiation

The inverse of the synchrotron energy-loss timescale for an escaping proton with Lorentz factor γ_p is

$$r_{p,syn} = t'^{-1}_{p,syn}(\gamma_p) = |\dot{\gamma}'_{p,syn}/\gamma'_p| = \frac{16}{3}\ c\sigma_{\rm T} n_0 \epsilon_B \Gamma\ (\frac{m_e}{m_p})^2\gamma_p$$

$$\cong 9.4 \times 10^{-6} n_2 \epsilon_{B-1} \Gamma_{300} E_{20} \, (\frac{\Gamma}{300}) \, \mathrm{s}^{-1} \, . \tag{27}$$

The mean proton synchrotron photon energy from escaping protons with energies $10^{20} E_{20}$ eV, $E_{20} = \gamma_{11}/10^{11}$, is given by

$$\epsilon_{p,syn} = \frac{3\Gamma}{1+z} \, \frac{B}{B_{cr}} \, \frac{m_e}{m_p} \, \gamma_p'^2 \, \cong 4.5 \times 10^5 \, \frac{\epsilon_{B-1} n_2 E_{20}^2}{1+z} \, , \tag{28}$$

notably independent of time. For parameters that make a highly radiative blast wave phase, $\epsilon_{p,syn}$ for proton synchrotron emissions from UHECRs in GRBs will be found in the TeV range with a well-defined spectrum ($a \cong 1/2$) to lower energies. To avoid attenuation by the diffuse intergalactic infrared radiation fields, low redshift GRBs measured are favored to detect this emission. These can be measured with low-threshold air Cherenkov telescopes such as MAGIC. The photon flux at these energies is very low, so only a few $\gtrsim 100$ GeV photons could be detected with a direct detection telescope such as GLAST.

3. Results

We adopt the following Standard Parameter set:

$$z = 1, \Gamma_{300} = 1, E_{54} = 1, n_2 = 1, \epsilon_{e-1} = 1, \epsilon_{B-1} = 1 \, .$$

This set is motivated by values that reproduce typical peak fluxes and durations for BATSE GRBs at $z \approx 1$ (Chiang & Dermer 1999), except that here $\epsilon_B = 0.1$ rather than $\epsilon_B \cong 10^{-4}$.

Fig. 1(a) plots the standard parameter rates for acceleration, photopion losses, proton synchrotron losses and escape for cosmic rays with energy $\bar{E}_p$, the νF_ν peak photon energy ϵ_{pk}, the cosmic-ray peak energy $\bar{E}_p$, and the mean proton synchrotron photon energy $\epsilon_{p,syn}$ radiated by protons with energy $\bar{E}_p$. Here and throughout we use an acceleration factor $\zeta_{acc} = 10$ and kinematic factor $k = 1$. The acceleration rate exceeds the inverse of available time throughout the early afterglow phase, so cosmic rays with energies $\sim \bar{E}_p$ are in principle easily accelerated through Fermi processes. Only at several hours into the afterglow emission do photopion losses limit acceleration to $E_p \lesssim \bar{E}_p$. At these late times, proton synchrotron emissions make a $\gtrsim$1% contribution to the total loss rate. The diffuse escape rate of protons can appear as a $\gtrsim$1% effect on the total rate, but is generally insignificant in the early afterglow. This GRB is brightest ≈ 20 s after first being detected.

The acceleration, escape, and loss rates for a cosmic ray proton with $E_p = 10^{20}$ eV are plotted in Fig. 1b. As can be seen, there isn't enough time to accelerate cosmic rays to

$\gtrsim 10^{20}$ eV energies for these parameters, so there can't be significant $\gtrsim 10^{20}$ eV cosmic ray (super-GZK) production or photopion losses from such GRBs. Protons would also escape before a significant fraction could be accelerated to such energies.

A set of parameters that overcomes these limitations is easily found. Consider Parameter Set 1,

$$z = 1, \Gamma_{300} = 1, E_{54} = 1, n_2 = 10, \epsilon_{e-1} = 3, \epsilon_{B-1} = 3 \ ,$$

giving the rates, fluxes, and energies shown in Fig. 2. For 10^{20} eV cosmic rays shown in the lower panel, an interesting conjunction occurs when $r_{\phi\pi} \approx 1/t'_{ava} \lesssim r_{acc}$, which happens here at ≈ 300 s. Protons accelerated to $\approx 10^{20}$ eV energies are converted, $\sim 1/3$ of the time, to ultrarelativistic neutrons that escape from the blast wave to form one component of a neutral beam (Atoyan & Dermer 2003), the other two components being the neutrinos and the γ rays.

The GRB formed in this example has a rather high $\epsilon_{pk} \sim 8$ MeV, but values of $\Gamma_0 \lesssim 300$ will lower ϵ_{pk} during the prompt phase and lengthen the prompt phase duration. Fig. 3 shows the results for Parameter Set 2

$$z = 1, \Gamma_{300} = 0.5, E_{54} = 10, n_2 = 10, \epsilon_{e-1} = 1, \epsilon_{B-1} = 3 \ .$$

This GRB peaks $\gtrsim 50$ s after the trigger, has a lower ϵ_{pk}, and reaches a slightly lower $f_{\epsilon_{pk}}$ peak flux than in Fig. 2. These correlations make a range of GRBs according to the variable-fireball-loading ("dirty-fireball") model (Dermer et al. 1999) for GRBs and X-ray flashes.

Parameter Set 1 gives a fast-cooling GRB with $\epsilon_e = 0.3$ and a radiative photopion phase. The 30% factor means that a large fraction of the swept-up power is assumed to be found in nonthermal electrons rather than in baryons or fields. A large body of parameter values clustering around the Parameter Set 1 values predict strong photopion losses in the early afterglow phase. If $\epsilon_e \lesssim 0.1$, then agreement with GRB energetics for the apparent total isotropic energy release means that any given GRB carries a large baryon load, so that $E_{54} \gtrsim 1 - 10$. The larger values of total apparent energy now acceptable due to a small ϵ_e parameter make it certain that, assuming that GRBs accelerate UHECRs, neutral beam power and escaping ions efficiently deplete internal blast wave energy and consequently affect the blast-wave dynamics.

4. Blast Wave Evolution from Radiative Discharge

Adiabatic expansion converts the internal energy of the explosion into directed kinetic energy. The equation of blast wave evolution is, according to Dermer & Humi (2001), given

by

$$-\frac{d\Gamma/dx}{\Gamma^2-1}=\frac{dm/dx+(\frac{\Gamma}{P^2})dU_{adi}/dx}{M_0+m(x)+U}\ , \tag{29}$$

where the blast wave momentum $P=\sqrt{\Gamma^2-1}$, $M_0=E_0/\Gamma_0 c^2$ is the initial baryon mass mixed into the explosion, and $m(x)$ is the swept-up mass. The quantity

$$U=m_p\int_0^\infty dp'(\gamma'_p-1)N'(p';x) \tag{30}$$

represents the internal energy, excluding rest-mass energy, where $p'=\gamma'^2-1$ is the proton's dimensionless momentum. The differential swept-up mass $dm(x)/dx=4\pi m_p x^2\ n_{ext}(x)$, and $n_{ext}(x)$ is the circumburst medium density, assumed radially symmetric about the GRB source. The internal energy U changes due to volume expansion according to the relation

$$\frac{dU_{adi}}{dx}=-\ m_p\ (\frac{1}{x}-\frac{1}{3}\frac{d\ln\Gamma}{dx})\ \int_0^\infty dp'\ (\frac{p'^2}{\gamma'_p})N'(p';x)\ . \tag{31}$$

The equations for the evolution of the blast-wave momentum $P=\beta\Gamma=\sqrt{\Gamma^2-1}$ are plotted in Fig. 4 in different approximations. The curve labeled "full treatment of adiabatic losses" uses the above equations. The curve labeled "momentum conservation solution" is the simpler equation

$$-\frac{d\Gamma/dx}{\Gamma^2-1}=\frac{dm/dx}{M_0+m(x)+U}\ , \tag{32}$$

where the adiabatic loss term is dropped, and which is often used to describe blast-wave evolution. As can be seen, this gives a reasonable approximation for relativistic blast waves. The curve labeled "analytic blast wave" is a plot of eq. (7), and the curve labeled "momentum conservation solution" shows the analytic form for a fully radiative blast wave (Blandford & McKee 1976; Chiang & Dermer 1999).

The intermediate curves are solutions to eq. (32) assuming that the internal energy in the blast wave is reduced by some fraction X of its original energy when the blast wave reaches $x=6\times10^{16}$. The light solid curves, from top to bottom, show $X=0, 25\%$, 50%, 75%, 90%, and 95%, with the 50% curve labeled. The 90% limit starts to represent the most rapid transition between radiative regimes possible.

This rapid radiative discharge drives the blast wave from a quasi-adiabatic regime into a strongly radiative regime, with an accompanying steep decline in the X-ray light curves,

thus explaining the Swift results (Tagliaferri et al. 2005; O'Brien et al. 2006). More detailed numerical simulations will be needed to assess the rapidity of the decline, which will be limited by the curvature effect (Kumar & Panaitescu 2000; Dermer 2004) unless the jet is structured. The temporal behavior of the escaping hadronic energy could also be responsible for the X-ray phase in the early afterglow that decays more slowly than predicted by the standard blast-wave physics model (Zhang et al. 2006; Fan & Piran 2006).

5. Explanations and Predictions

5.1. Explanations

Up to now, the details of the acceleration mechanism remain sketchy. The derivation of the acceleration rate, eq. (22), considered only the shock fluid quantities, and so is commensurate with a turbulent, stochastic Fermi Type 2 mechanism, for example, through gyroresonant acceleration of ions and electrons via MHD wave turbulence. Acceleration through the stochastic Fermi mechanism makes hard number spectra ($n(\gamma) \propto \gamma^{-1}$), with most of the energy content in the highest particle energies (Dermer & Humi 2001). Under these circumstances, the cosmic-ray neutron discharge from GRB blast waves, as considered here, produces a component of the UHECRs, possibly the dominant one. The mean injection spectrum per GRB is not yet calculated, and could range from a flat $\gamma^2 n(\gamma)$ over a narrow energy range, as in the model of Waxman & Bahcall (1999), to a power-law injection $\gamma^2 n(\gamma) \propto \gamma^{-0.2}$, as in the model by Wick et al. (2004).

The release of energy in the form of neutrons or escaping ions means that there was much more energy in the GRB blast wave during the prompt phase. Thus the efficiency of γ-ray production during this phase is low, which reduces the requirements on efficiency in either external or internal shock models of GRBs.

5.2. Predictions

Here we discuss direct, radiative signatures for the hypothesis that UHECRs originate from GRBs. Figs. 2 and 3 show conditions where rapid dissipation of hadronic energy through photopion processes happens. In all cases, the blast wave is assumed to be radiating in the fast-cooling limit, so that the νF_ν indices $a \cong 1/2$ and $b = 1 - (s/2)$, where s is the electron injection index (with $s \approx 2.2$ for shock Fermi models). Already a careful spectral analysis when ϵ_{pk} sweeps through the Swift XRT detector could see if GRB blast waves evolve within a few hundred seconds to a condition where the ϵ_e and ϵ_B parameters are each $\gtrsim 10\%$.

GLAST GBM and LAT observations joint with Swift will reveal the details of GRB spectral evolution in exquisite detail. For the external shock model considered here, the smooth circumburst medium asymptote is the easiest to calculate and gives typical values for GRB emission properties. The temporally evolving ϵ_{pk} can be measured with GLAST GBM and Swift BAT and XRT for comparison with generic external-shock model expectations, as shown in Figs. 1 – 3. Differences between smooth profile and structured GRBs are due to interactions of the thin blast wave with circumburst clouds having densities $\gtrsim 10^3$ cm^{-3} and sizes $\lesssim x/\Gamma$. In the external shock model, the GRB image consisting of γ-ray pulses and X-ray flares is the tomographic image of the circumburst density along the line-of-sight to the GRB explosion center (Dermer & Mitman 1999), not the consequence of internal shell collisions.

A prediction of this model is hadronic γ-ray light consisting of proton synchrotron, photopion and secondary photohadronic decay radiations that cascade to low enough energies that $\gamma\gamma$ pair attenuation processes become negligible. This component varies differently from the X-ray lepton synchrotron component, as demonstrated here for an adiabatic blast wave. According to this interpretation, the hadronic emission component was already evident in GRB 940217 (Hurley et al. 1994) and GRB 941017 (González et al. 2003), though some of the γ rays for GRB 940217 may be SSC photons and some are background. The independently varying hadronic emission component is a prediction for GLAST, and a major test of this model.

Strong TeV radiations are made by the proton synchrotron and photopion cascade radiations. The onset of strong photohadronic processes during the afterglow phase might explain why the highest energy photon from GRB 941017 was seen ≈ 90 min after the GRB (Hurley et al. 1994). As a prediction for the GLAST LAT, this model implies that anomalous high energy γ rays from photohadronic processes should appear at $\sim$ minutes to hours after the start of a GRB.

Ultra-high energy neutrinos are made by the release of blast wave energy though this mechanism, and we predict the detection of a delayed neutrino flux at high energy. Unfortunately the $\gtrsim 10^{17}$ eV neutrinos from the photohadronic processes in GRB blast waves are at a difficult energy for IceCube to detect, but the $\gtrsim 10^{18}$ eV neutrinos could be detected in sideways showers with Auger, or in balloon-borne detectors such as ANITA. The prediction of the PeV neutrino flux for external shock processes in the prompt phase have only been made for a uniform surroundings, where the rate is too low to be detectable with IceCube (Dermer 2002). A clumpy medium may improve detectability; this has not been calculated yet. But in the internal shell model for the γ-rays during the prompt phase, UHECRs accelerated in large fluence GRBs make neutrinos that would be detectable with IceCube when

the shocked shell Lorentz factors ≈ 100, while being optically thick to $\gamma\gamma$ attenuation at GeV energies (Dermer & Atoyan 2003; Razzaque et al. 2004; Guetta et al. 2004).

If GRBs are the progenitors of UHECRs (Waxman 1995; Vietri 1995; Dermer 2002), then the superposed cosmic-ray intensity spectrum from all the UHECR GRB sources over cosmic time display features of propagation: most pronounced are the GZK feature and the ankle feature, possibly due to pair production (Berezinskii & Grigor'eva 1988; Wick et al. 2004; Berezinsky et al. 2005). Thus the UHECR spectrum will trace the GRB formation rate, which could be different than the star formation rate due to metallicity-dependent effects and the population of high-mass stars that collapse to form GRBs.

6. Summary and Conclusions

By carrying through the analysis of a complete leptonic/hadronic GRB blast-wave model, we found a region of parameter space where, even in the simplest constant density blast-wave model, photohadronic processes have important effects on blast-wave evolution. Hadronic emissions consisting of high-energy neutrinos, cascade γ rays, and escaping cosmic-ray neutrons are made by photopion processes, and additional cascade γ rays are made by proton synchrotron radiation. This happens a few hundred seconds after the start of the GRB for circumburst medium densities $n_0 \gtrsim 10^2$ cm^{-3}, $100 \lesssim \Gamma_0 \lesssim 300$, $E_{54} \sim 1$ – 10, and $\epsilon_e, \epsilon_B \gtrsim 10\%$.

The GRB blast wave is predicted to evolve toward the strong cooling regime in the early afterglow due to a strong photohadronic discharge of energy and direct escape of UHECR ions. The change of ϵ_{pk} with time may indicate the evolution of the radiative regime during the prompt and early afterglow phases. Hadronic γ-ray emission components are expected in the early afterglow and extending to $\gtrsim 10^4$ s after the GRB. The hadronic emission is generally independent of the X-ray lepton sychrotron emission, but could be brightest during the epoch where the most rapid X-ray declines are measured. A related flux of $\gtrsim 10^{17}$ eV neutrinos is made at this time.

UHECRs originate from the hadronic discharge of ultra-high energy neutrons formed in charge-changing photopion reactions and from escaping UHECR protons and ions. Detection of photohadronic neutrinos and GeV – TeV γ rays in the early afterglow is a crucial test of this model for cosmic-ray origin.

I thank A. Atoyan, M. Böttcher, and J. Chiang for collaboration and comments. I also thank Dr. E. Nakar for pointing out how this solution could resolve efficiency concerns in

GRB models. This work is supported by the Office of Naval Research, by NASA *GLAST* Science Investigation No. DPR-S-1563-Y, and NASA Swift Guest Investigator Grant No. DPR-NNG05ED41I.

REFERENCES

Atoyan, A. M., & Dermer, C. D. 2003, ApJ, 586, 79

Berezinskii, V. S., & Grigor'eva, S. I. 1988, A&A, 199, 1

Berezinsky, V., Gazizov, A. Z., & Grigorieva, S. I. 2005, Physics Letters B, 612, 147

Blandford, R. D., & McKee, C. F. 1976, Physics of Fluids, 19, 1130

Böttcher, M., & Dermer, C. D. 1998, ApJ, 499, L131

Böttcher, M., & Dermer, C. D. 2000, ApJ, 532, 281

Chiang, J., & Dermer, C. D. 1999, ApJ, 512, 699

Dermer, C. D., Chiang, J., Böttcher, M. 1999, ApJ, 513, 656

Dermer, C. D. 2002, ApJ, 574, 65

Dermer, C. D. 2004, ApJ, 614, 284

Dermer, C. D., & Atoyan, A. 2003, Physical Review Letters, 91, 071102

Dermer, C. D., & Humi, M. 2001, ApJ, 556, 479

Dermer, C. D., & Mitman, K. E. 1999, ApJ, 513, L5

Fan, Y., & Piran, T. 2006, MNRAS, 369, 197

Gehrels, N., et al. 2004, ApJ, 611, 1005

González, M. M., Dingus, B. L., Kaneko, Y., Preece, R. D., Dermer, C. D., & Briggs, M. S. 2003, Nature, 424, 749

Guetta, D., Hooper, D., Alvarez-Mun˜iz, J., Halzen, F., & Reuveni, E. 2004, Astroparticle Physics, 20, 429

Hillas, A. M. 1984, ARA&A, 22, 425

Hurley, K. 1994, Nature, 372, 652

Kumar, P., & Panaitescu, A. 2000, ApJ, 541, L51

Mészáros, P. 2006, Rep. Prog. Phys. (astro-ph/0605208)

Mészáros, P., & Rees, M. J. 1993, ApJ, 405, 278

O'Brien, P. T., et al., 2006, ApJ, in press (astro-ph/0601125)

Panaitescu, A., & Mészáros, P. 1999, ApJ, 526, 707

Piran, T. 1999, Phys. Reports, 314, 575

Rachen, J. P., & Mészáros, P. 1998, Phys. Rev. D, 58, 123005

Razzaque, S., Mészáros, P., & Zhang, B. 2004, ApJ, 613, 1072

Sari, R., Piran, T., & Narayan, R. 1998, ApJ, 497, L17

Tagliaferri, G., et al., 2005, Nature, 436, 985

Vietri, M. 1995, ApJ, 453, 883

Vietri, M. 1998, ApJ, 507, 40

Waxman, E. 1995, Physical Review Letters, 75, 386

Waxman, E., & Bahcall, J. 1999, Phys. Rev. D, 59, 023002

Wick, S. D., Dermer, C. D., & Atoyan, A. 2004, Astroparticle Physics, 21, 125

Zhang, B., Fan, Y. Z., Dyks, J., Kobayashi, S., Mészáros, P., Burrows, D. N., Nousek, J. A., & Gehrels, N. 2006, ApJ, 642, 354

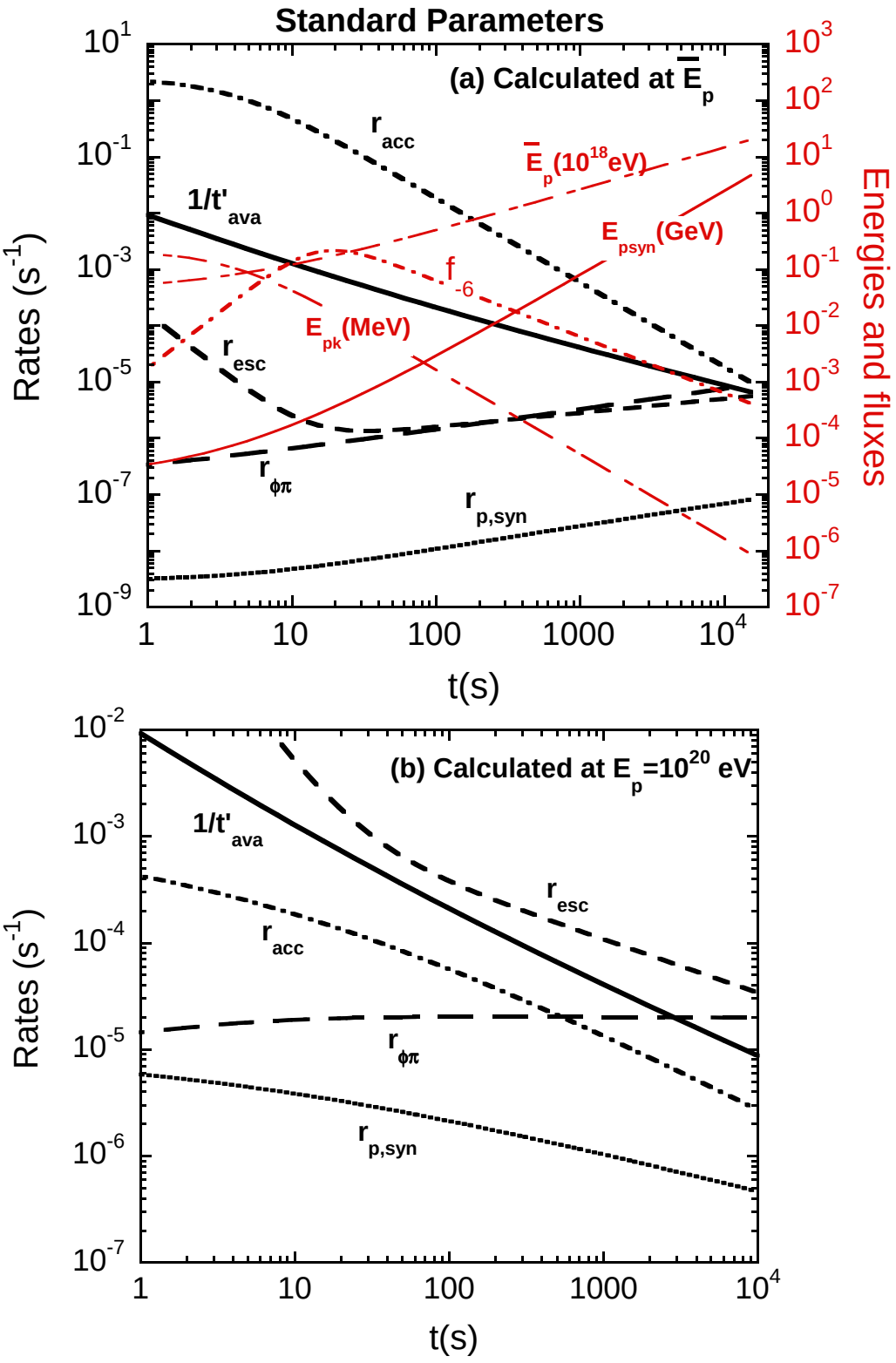

Fig. 1.— (a) Characteristic rates and energies calculated at $\bar{E}_p$, (b) characteristic rates calculated at $E_p = 10^{20}$ eV, using the Standard Parameter set.

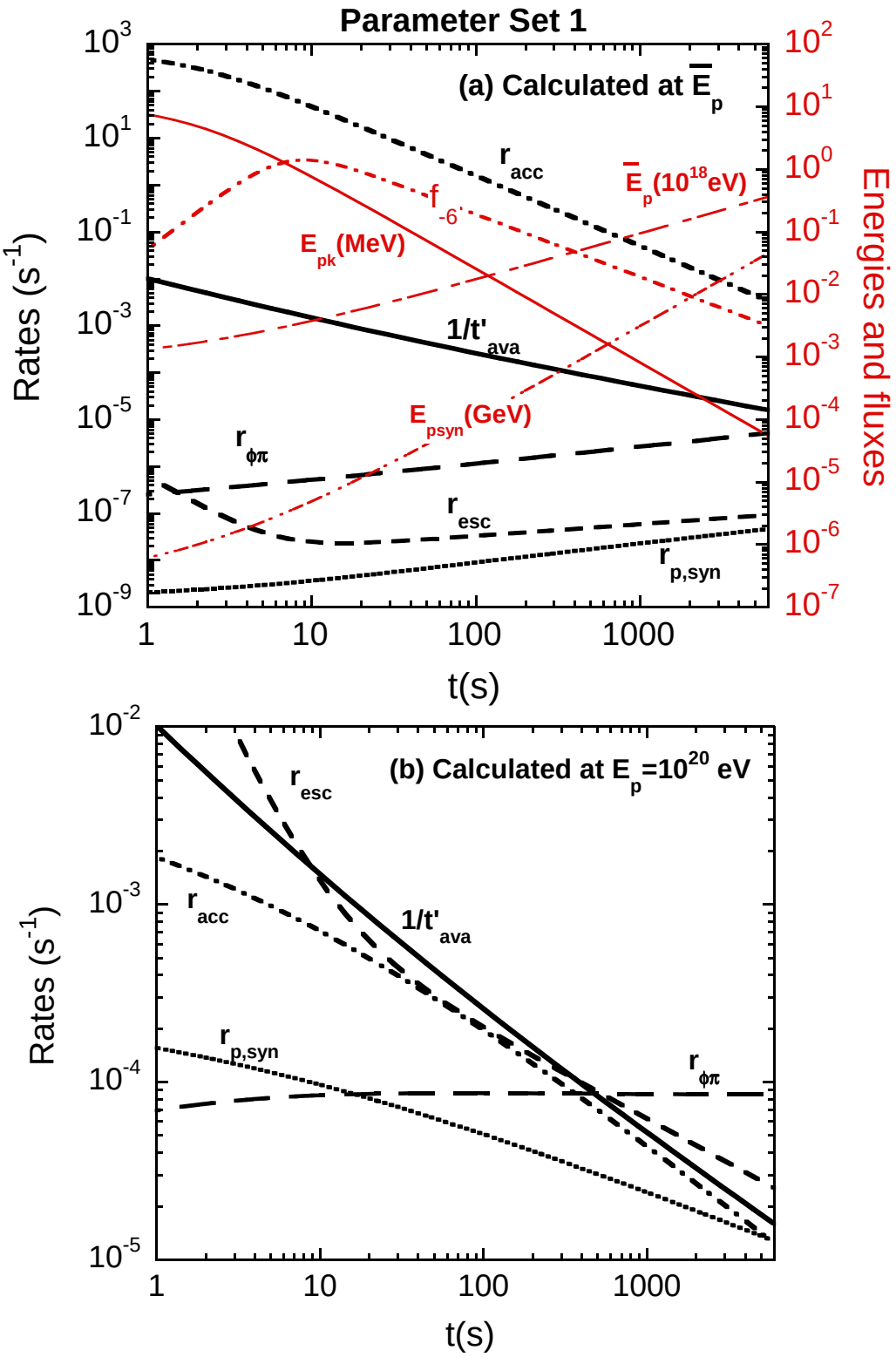

Fig. 2.— As in Fig. 1, but calculated for Parameter Set 1, with the energy of electrons, protons, and magnetic field in approximate equipartition.

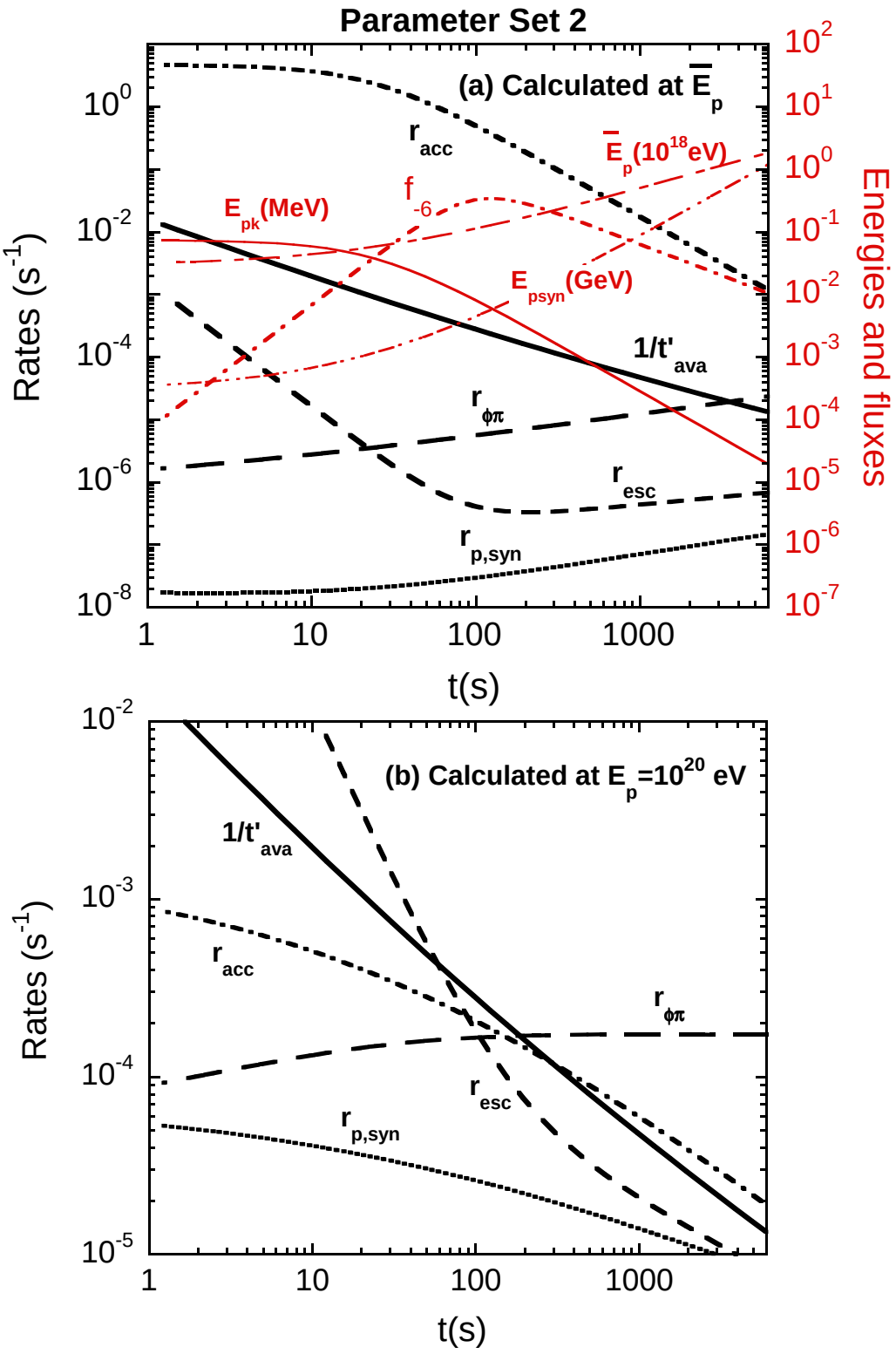

Fig. 3.— As in Fig. 1, but calculated for Parameter Set 2.

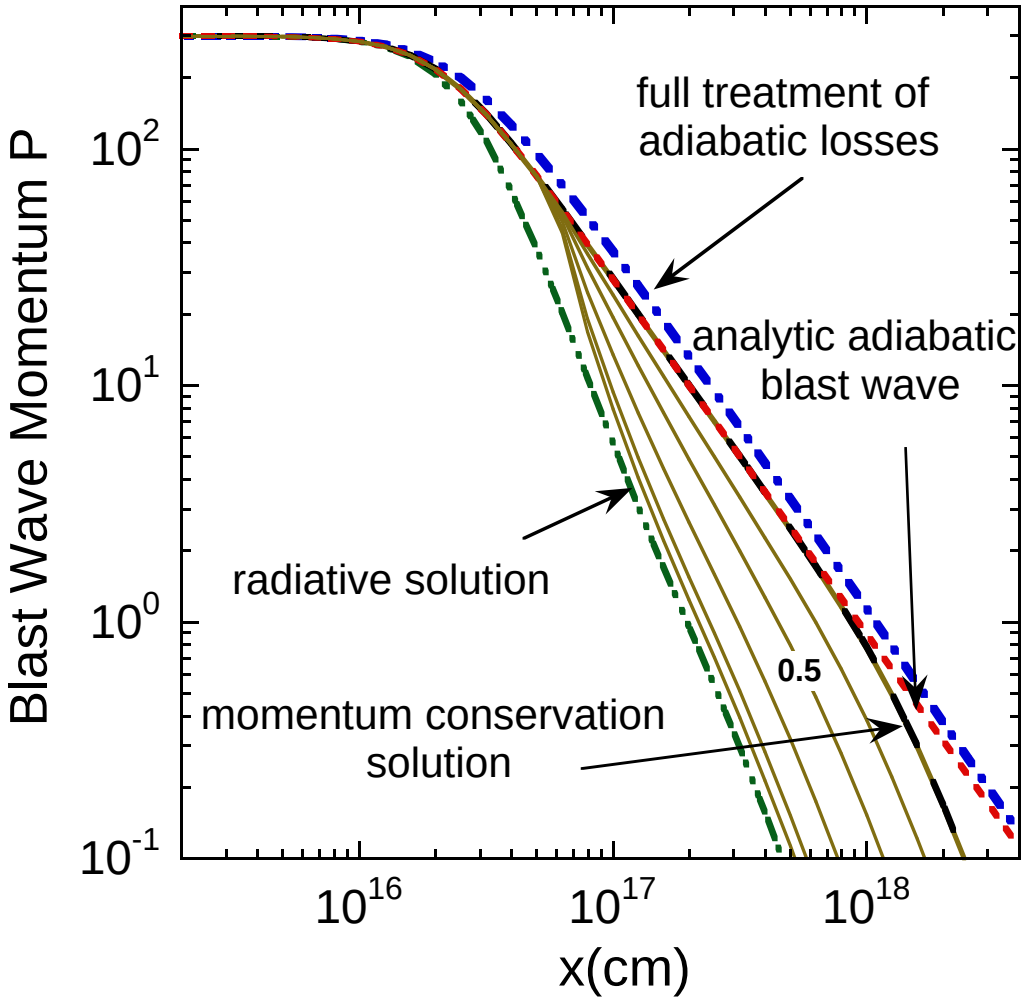

Fig. 4.— Evolution of GRB blast wave in different approximations (see text).